Optimized Design and Implementation of Digital Lock-In for Planetary Exploration Sensors

Alberto Ramírez Bárcenas, Rolando Paz Herrera, Jose A. Miranda Calero, *Member, IEEE*, Manuel F. Canabal, Ernesto García Ares, Andres Russu, Francisco Cortés, Antonio J. de Castro, Fernando López, Marta Portela-García, and Celia Lopez-Ongil, *Senior Member, IEEE*

***Abstract*—Exploring life conditions on the near-Earth planets and satellites before carrying out human missions is an important task for space agencies. For that purpose, scientific space missions usually include instruments to measure climatological variables. Within this space instrumentation and measurement context, dust sensors (DSs) aim to measure dust particles in suspension and provide valuable information for persons and equipment life conditions, while they must deal with low signal-to-noise ratios (SNRs). For example, the Exomars mission is focused to characterize the weather on Mars surface and include up to four DSs based on different technologies: infrared (IR), laser, interferometry, impact sensors, and electric field activity sensors. Due to the tight budget in terms of area, weight, power consumption, and data budget in aerospace instruments, as well as ionizing radiation and extreme temperatures, current solutions present low scalability and configurability. In this article, a novel system proposal that extracts valuable information from noisy signals obtained from IR sensors aimed to measure airborne dust is presented. The solution provides competitive capabilities in terms of power consumption, data budget, SNR, and reconfigurability. It has been implemented in a rad-hard Microsemi field programmable gate array (FPGA) (RT54SX32S). Therefore, robustness and scalability are guaranteed. The results reported a maximum power consumption of up to 141 mA (@12 Vdc), a sensitivity of 19.5 mV (input signal), and a data budget of 32 B/s. This research possesses great potential to further instruments not only in planetary exploration but also at Earth applications.**

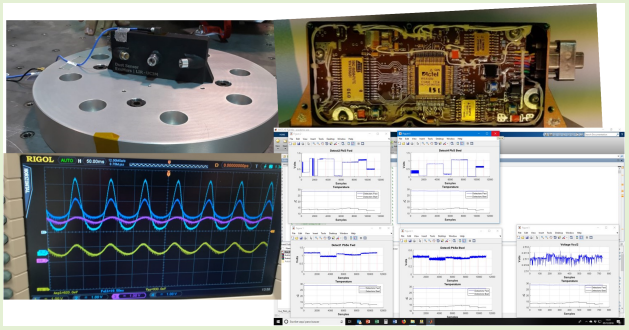

***Index Terms*—Computing on-the-edge, digital lock-in (LI) amplifier, dust particles, field programmable gate array (FPGA), infrared (IR) sensors, Mars exploration.**

I. Introduction

SPACE exploration has always been a challenge for humanity and science. In 1957, the launch of the artificial satellite Sputnik marked the beginning of a race to unravel the mysteries that surround us [1], [2]. The need to collect samples, develop hypotheses, and test theories necessarily goes through planetary exploration. Currently, the technology has advanced enough to venture into the surrounding space, even so, due to the unusual characteristics, there are several limitations and drawbacks to be tackled. Typical tasks, such as power generation and data transmission, are trivial processes on Earth but require a higher level of complexity in planetary exploration. This fact, added to other drawbacks such as ionizing radiation, lack of a medium to evacuate the heat, and the extreme operating conditions (vacuum, extreme temperatures, effects of vibration in the takeoff, and landing impact), poses very strict methodology and procedure of design, testing, and implementation in the generation of electronic components embedded in satellites, spacecraft, and space probes [3], [4], [5].

Since the beginning of the space exploration career, many measurement instruments have been designed to characterize the unexplored environment by collecting samples and transmitting data for analysis. However, it was not until the

Manuscript received 14 July 2022; revised 22 September 2022; accepted 26 September 2022. Date of publication 17 October 2022; date of current version 30 November 2022. This work has been partially supported by the Ministry of Science, Innovation and Universities of Spanish Government, in the research projects INMARS-RTI2018-099825-B-C33 and ESP2015-67624-R and by the Madrid Government (Comunidad de Madrid-Spain) under the Multiannual Agreement with UC3M in the line of Excellence of University Professors (EPUC3M26), and in the context of the V PRICIT (Regional Programme of Research and Techno-logical Innovation). The associate editor coordinating the review of this article and approving it for publication was Dr. Pu (Perry) Wang. *(Corresponding author: Celia Lopez-Ongil.)*

Alberto Ramírez Bárcenas, Rolando Paz Herrera, Jose A. Miranda Calero, Manuel F. Canabal, Marta Portela-García, and Celia Lopez-Ongil are with Electronic Technology Department, Universidad Carlos III de Madrid, 28911 Madrid, Spain (e-mail: alramire@ing.uc3m.es; celia@ing.uc3m.es).

Ernesto García Ares is with the Technical Office, Universidad Carlos III de Madrid, 28911 Madrid, Spain.

Andres Russu, Francisco Cortés, Antonio J. de Castro, and Fernando López are with the Infrared Laboratory, Physics Department, Universidad Carlos III de Madrid, 28911 Madrid, Spain.

Digital Object Identifier 10.1109/JSEN.2022.3213423

21st century that coordinated actions between different space agencies in the field of planetary exploration were carried out. For instance, MARS 2020 is a mission run by National Aeronautics and Space Administration (NASA) focused on exploring the surface of Mars planet [6]. Within the European context and run by both European Space Agency (ESA) and Roscosmos Space Agency, the EXOMARS mission aims to investigate the possible signs of life on Mars and explore its environment [7]. This mission comprised a rover, which would search for signs of past and present life by geological analysis, and a surface platform (SP), which would study Mars' weather at the surface level with several instruments [7].

METEO is the Meteorological Package in the SP under responsibility of the Russian Space Research Institute, Institut Kosmicheskikh Issledovaniy (IKI), Moscow, Russia. Most of the weather instruments included in the platform are designed and implemented by European research centers. One of these instruments is the Radiation and Dust Sensors Module (RDM), which is supervised by the National Institute of Aerospace Techniques (INTA), Spain. The proof of concept of the research presented in this article is the UC3M Dust Sensor, which has been designed by the Universidad Carlos III de Madrid (Spain) and manufactured at INTA facilities.

Obtaining meteorological variables on Mars is a task of maximum interest in the field of planetary exploration. In fact, the analysis of airborne dust is of special attention to characterizing the environment on this planet. Airborne dust in the Martian atmosphere is a key factor to consider in the presence of life and/or instrumentation. Both, suspended and transported dust through the air, can harm in terms of health and degradation of elements. This dust reflects and absorbs solar radiation, being responsible for influencing various phenomena such as heat exchange with the planetary surface or visibility. Dust storms can be especially harmful to any instrument, and its deposition and their electrostatic nature can cause failures and malfunctions [8], [9], [10], [11]. An instrument working on Mars' surface in the Oxia Planum region must work under very hard conditions: temperatures ranging from -90 °C to -10 °C [12], ionizing radiation due to the lack of magnetosphere, low atmospheric pressure, and so on. This scenario is getting more complex when data from many different instruments should pass through the same data link: the gateway node and the planet orbiter. On this basis, UC3M Dust Sensor is conceived for the remote sensing of parameters that define the size distribution function of the airborne dust in the Martian atmosphere. These measurements have a surface and local character.

Fig. 1 shows a schema of the instrument. A hot infrared (IR) source emits radiation that it is scattered by the dust particles inside the interaction volume. This scattered radiation, which depends on the wavelength and the scattering direction, is measured by four IR detectors. Two of these detectors are lead sulfide (PbS) detectors and sensitive in the 1–3-μm spectral region. The other two detectors are lead selenide (PbSe) detectors, sensitive in the 3–5-μm spectral region. Every type of detector is located at two different positions to correctly detect the forward and backward scattering. Note that this nomenclature corresponds to the incident angle regarding the light beam axis of the IR source and the central axis of the field

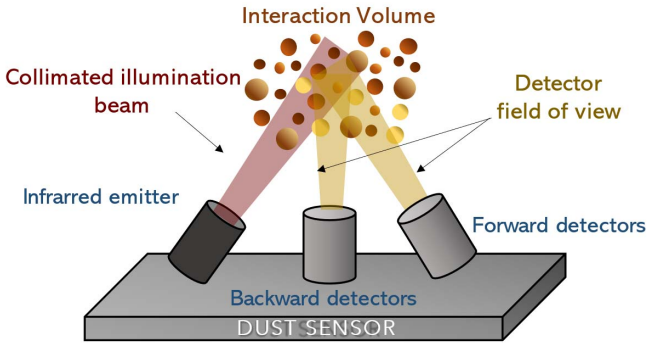

Fig. 1. DS working principle.

of view of each detector, in the range of 0°–90° for the forward detectors and 90°–180° for the backward detectors [13].

In the space exploration missions, low power consumption, low weight, and small area, short processing time, high robustness, and high efficiency in communication and processing tasks are critical aspects to comply with. Unnecessary data processing and/or communication is avoided to improve the performance and meet aerospace instrument specifications. However, sensor's signals should be sampled with enough resolution to obtain representative measurements of the magnitude under analysis with high signal-to-noise ratios (SNRs). Thus, digital signal processing techniques are embedded in the electronic part of the instruments to clean noisy signals and extract valuable information.

Generally, most acquired signals present short ranges in their values and, in many cases, the environment couple significant noise levels compared to the signal of interest, apart from the noise due to the acquisition channel [14]. Another added problem is due to the outdoor operation of the instrument, where it can exist signals within the frequency spectrum of interest. Other IR sources, such as the Sun radiation received on Mars' surface, may interfere as another IR emitter. This radiation can reflect on the surfaces of the instrument itself, creating multipath, heating the material, and provoking additional electromagnetic waves that can be received and interpreted as spurious signals and noise in data analysis [15]. In these cases, where the SNR values are so degraded, it is necessary to apply techniques to recover the signal from the background noise, as will be considered in the rest of the paper.

Characteristics, such as high robustness against ionizing radiation and the others mentioned above, must be met by the instrument [16], [17]. For this reason, space-qualified components are required as well as specific manufacturing and mounting techniques to assure support for the harsh conditions of working (temperature, vacuum, and radiation). Besides, digital signal processing should comply with fault tolerance requirements, and hardware, time, and/or software redundancy will add extra complexity in terms of performance while assuring data integrity and system robustness. This is especially critical for multisignal processing. It can be implemented in rad-hard or rad-tolerant modules, either in a customized device [field programmable gate array (FPGA) and Applications Specific Integrated Circuit (ASIC)] or in a microprocessor, which may imply a longer processing time [18], [19].

Processing digitalized measurements *on-the-edge* allows for detecting and correcting errors and extracting only the valuable information prior to data transfer. Efficient signal data processing is one of the main objectives throughout the EXOMARS mission. Complex mathematical operations should be combined with the smallest word lengths, fewest operators, and memory blocks as possible without losing accurateness.

This article describes the digital signal processing architecture proposed, designed, and implemented for the "DS" multisensor dust detection instrument. A digital lock-in (LI) has been designed, implemented, and time multiplexed to manage the signals received from the four IR sensors. The proposed system is able to generate a 10-Hz sinusoidal signal to excite the IR emitter; to get data from four IR integrated sensors (previously analog filtering and amplifying them), at a sample rate of 1 kHz per every sensor; to extract Vp (voltage peak) of every IR signal, which is the most intensive processing task (two values per second, enough data rate for long-term monitoring of Mars airborne dust); and to retrieve this information. During data acquisition, approximately 4.6 MB of data per hour are received from the four detectors (also, housekeeping data are received regarding temperature and voltage). After data processing, 19.25 kB of data per hour, regarding IR sensors, are sent in 4.03 s upward.

II. Signals in Space Missions: Related Work

The SNR is the parameter that defines the ability to detect a message above the noise at reception and the most important index to measure the channel communications quality [20]. An SNR close to 1 implies that noise and signal are presenting similar power levels; thus, it would be highly unlikely to extract the useful information received using the conventional approaches.

There are several methods proposed in the literature to solve this problem. The use of redundancy is the most straightforward. If the message is repeated several times in a noisy environment, the probability of making an error in the reading of real data is lower, so the SNR will increase. This achieves a better chance of decrypting the message at the source, but, consequently, the throughput data decrease [21]. A redundant method by hardware is the concurrent use of several sensors, but in many practical cases, it is not a good solution, requiring a larger design, with more components and power consumption [22].

Differential sensing, so as the noise is canceled in common mode, is explained in [23], increasing the SNR parameter. It is used in standards of digital communications, such as Ethernet and RS485, and their principal advantage is the robustness against the common-mode noise.

It is also possible to cancel the ambient noise by making use of two sensors where one is slightly closer to the source, although both capture noise simultaneously. The use of this principle can be observed in the active noise cancellation (ANC) techniques [24], [25], [26]. This technique is widely used in mobile phone microphones for noise cancellation.

Another method reported in the literature is the signal regeneration, which is widely used in radio communications and requires an intermediate signal treatment to improve the SNR. In radio, the use of a superheterodyne receiver is also used for high-frequency signals where the signal is amplified and filtered with low selectivity at the beginning of the channel and then mixed and taken to a lower intermediate frequency to eliminate noise at low frequencies, filter with greater selectivity, and perform better signal processing [27], [28].

For signals obtained from sensors with very low amplitude output values (normally voltages or currents), the LI amplification is widely recommended. The noise in these sensors highly impregnates the weak signal, degrading the SNR parameter, making it very difficult to extract its characteristics. This technique is based on phase-sensitive detection, and the amplitude and phase parameters of a low-power signal, masked with noise, can be extracted. Phase-sensitive detection is an important concept in signal recovery from a noisy environment, and sampling itself requires a good SNR figure, so the use of the LI technique will play an important role [13].

The use of phase-sensitive detection has long been used in a versatile way to extract low levels of noise-masked signals. This concept was documented by researchers in the late 1960s [29] and used in a variety of applications using analog electronics with the technology available at the time [30]. To achieve vector tracking, the concept of "two-phase LI" was introduced into the system [31]. With the advance of microprocessors and digital microelectronics, digital processing of sensor data, due to analog to digital converters (ADCs) and DACs conversion, became more efficient and mixed designs began to be implemented [29], [30], [31]. In these first approaches, the generation of the reference signal was carried out with analog ICs and the processing was done in the digital domain [32], [33], [34], [35], [36], [37].

With the LI technique, some applications have been developed for the sensing of biological variables, for the sensing of gases even in thermography for the revision of aerospace equipment [32], [38]. However, in the field of planetary exploration, it has not been widely deployed because, until recently, the LI used in sensor interfaces was not portable or flexible enough for their use. Fortunately, the digital implementation of LI technique is possible nowadays in devices such as FPGA [32], [39]. Even so, up to our knowledge, there is no instrument in any space exploration mission that applies the LI technique for the acquisition of a noisy signal, optimized for area, power consumption, and high efficiency.

A. DSs Instruments for Planetary Explorations

As mentioned in Section I, dust measurement is a key factor in space exploration, specifically to characterize the weather conditions in Mars planet. In the aerospace industry, there are already instruments for measuring the airborne suspended dust. Some of them have been already designed and prototyped and others are still in their development phase. The most significant examples are given as follows.

1) Grain Impact Analyzer and Dust Accumulator (GIADA) designed to measure the evolution of comet dust flow and the dynamic properties of dust grains. It was integrated in the "Rosetta" mission, from ESA [40].

2) Martian Atmospheric Grain Observer (MAGO) devoted to measuring the physical properties of dust grains, provided by another instrument in charge of taking a portion of soil, processing it, and delivering it for analysis. Similar to the previous instrument, it makes use of a micro-balanced system (MBS) and a grain detection system (GDS) added to an impact sensor (IS) to provide a quantitative measurement of mass and size distribution of dust particles [41]. This instrument was supported by the Italian Space Agency.
3) Martian Environmental Dust Systematic Analyzer (MEDUSA) is an instrument that studies dust and water vapor in the low Martian atmosphere. It focuses on measuring the properties of a single intercepted particle with a diameter between a few units to hundreds of micrometers. It requires a pump to drag the dust inside a chamber and a laser diode as an active device, with a group of detectors, as well as a micro-balanced quartz crystal; also, Peltier temperature control for the sensing of water vapor is included [42], [43].
4) MicroMED is a miniaturized version of MEDUSA, which has been designed and prototyped for the Humboldt payload in the EXOMARS mission [42], [44] (ESA), by a consortium of Spanish National Institute of Aerospace Techniques and Italian research institutes taking into the base the MEDUSA heritage [42], [43], [45].

UC3M Dust Sensor, whose physical principle was presented in [13] and outlined in Section I, presents some differences with these previously detailed instruments, which can make it interesting for monitoring large areas on the planet's surface with low cost, low power consumption, and acceptable data budget for telemetries. DS is based on IR emitter and four IR detectors working at ambient temperature, with neither mobile parts nor temperature control. The implementation of a digital LI, with signal oversampling, has been done on a time multiplexed architecture, with short data widths and resources sharing, providing accurate results for the four IR detectors with a low data budget. These data can be post-processed at-Earth to extract the characteristics of the observed airborne dust particles. Although effective measurement volume is close to the instrument itself, its low cost can make possible the spread of many of them in wide areas.

Although LI is a well-known technique, in this work, a digital architecture is designed and implemented for processing real-time signals (there is no memory to store samples) from four sensors within a constrained and small embedded device (1080 DFF and 1800 combinational blocks) and with the possibility of changing the carrier frequency with the same hardware. This architecture is detailed in Section III.

III. System Description

The DS system is composed of different subsystems that perform the functions of detection, signal conditioning and processing, as well as system control and results from data transmission. An outline of the main parts of the system is shown in Fig. 2.

As previously explained, the working principle of the DS system is based on the active detection of dust by scattering

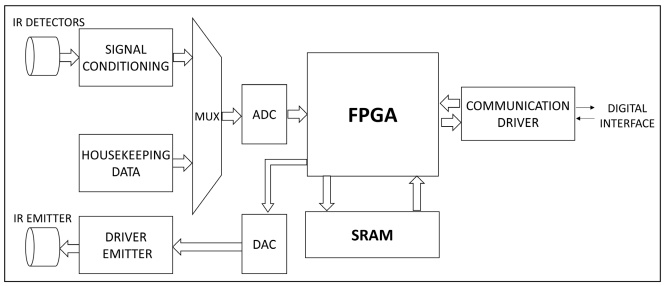

Fig. 2. DS general scheme.

IR light. For this purpose, the system uses an IR source excited with a low-frequency modulated signal in the carrier frequency of interest (10 Hz) and a dc component. The working bandwidth of the emitting source limits the range of carrier frequencies that can be used without decreasing its modulation depth. The purpose of exciting the IR source with a frequency signal is to extend its lifetime to guarantee its operation during the whole mission time.

The system detects the light scattered by dust particles with four IR detectors arranged in two positions under the study area: in one of them, the scattered light is captured, when it hits the dust cloud, in the "forward" direction and in the other in the "backward" direction, Fig. 1. Each position integrates two IR active detectors, which are PbSe and polycrystalline PbS that work in the range of 3–5 μm and 1.3–2.6 μm, respectively. The micrometer-sized suspended particles that are an important component of the Martian dust will scatter with a great efficiency the IR light emitted by the DS source. This scattered light depends strongly not only on the radiation wavelength but also on the scattering angle. DS has been designed to take advantages on these spatial and spectral dependences. Signal ratios measured at the two spectral bands in the two spatial directions will be used as inputs of a retrieval model, which provides the characteristic parameters of the size distribution. Materials are covered with a filter for spectral band spacing. The intensity of the light, produced by the scattering, incident in the "forward" direction depends mainly on the angle of incidence and the particle size, while in the "backward" direction, it will also depend on the refractive index of the particle material. Optimal scattering light detection should include both "backward" and "forward" detections for a complete analysis [13].

The system has an analog front end to stimulate the IR emitter and to filter and amplify the IR sensed signals. In addition, the system collects housekeeping data: the temperature in the detectors and in the board, as well as the analog supply voltage. The detected IR signals, together with the housekeeping information, are converted to digital values. A single 16-bit ADC (Maxwell Technologies' 7809LP) is used, fed by an analog multiplexer digitally controlled at a 1-kHz frequency (ST's M54HC4051), which interfaces with the digital module through a serial protocol (@2 MHz). Both components are rad-hard. The digital module is implemented in an antifuse rad-hard Microsemi[1] FPGA (RT54SX32S) and a

[1]Registered trademark.

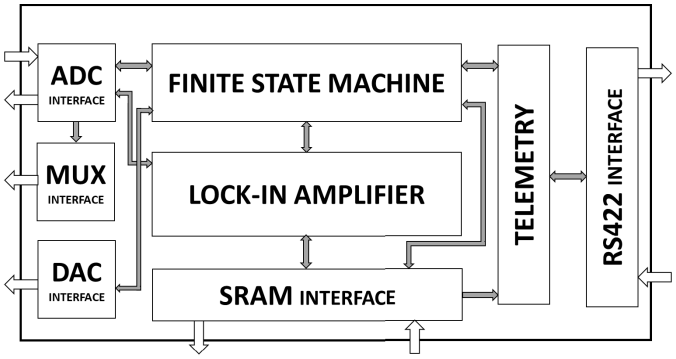

Fig. 3. Digital circuit scheme in the FPGA.

rad-hard static random access memory (sRAM) 1 Mbit memory for storing temporary and final data (Atmel's M65608E).

In the system, the behavior itself of IR detectors incorporates a noise level, just like analog electronics, which is added to the noise perceived in the IR spectrum captured in the measurement environment. To deal with the unwanted signals produced, the LI technique eliminates any frequency component outside the one of interest and captures the utility parameters that characterize the signal under study. The FPGA implements this LI in a digital architecture that is applied to the four sensors' data in time-multiplexed scheduling. The outputs of this LI are the Vp and phase values of the four IR sensed signals (two results per second).

In addition, the FPGA generates the excitation signal of the IR emitter, which is sent to a DAC block. This DAC (Texas Instruments' DAC121S101QML-SP) has a resolution of 10 bits. Finally, the control and telemetry functionality are also implemented within this FPGA through a finite-state machine (FSM) and RS-422 serial interface (Intersil's HS-26CT31RH). A scheme of the digital circuit implemented in the FPGA is shown in Fig. 3.

The DS instrument must respond to commands sent from a central control module called CEU (central electronic unit), with the requirements established for the set of instrument packages. Through an RS422 communication serial interface, the METEO CEU can send control and telemetry commands to retrieve the data relative to Vp and phase obtained by the digital processing implemented and stored in the digital module, together with the housekeeping information. The DS can be activated every hour to measure for ten Martian minutes and deliver two samples per second (1232 samples per measurement channel per campaign), in the general case; also, other type of measurements can be programmed.

The digital architecture of the system was described in VHDL language to assure technology independence, including various configurable parameters for the sake of flexible further implementations. These parameters are the number of input channels, the frequency of signal carrier, the filter cutting frequencies, amplitude, and the reference wave type, which can be changed without suffering the cost of system redesign and area optimization. Besides, efficient parameterizable filters for the digital LI have been designed and implemented with the least number of resources possible.

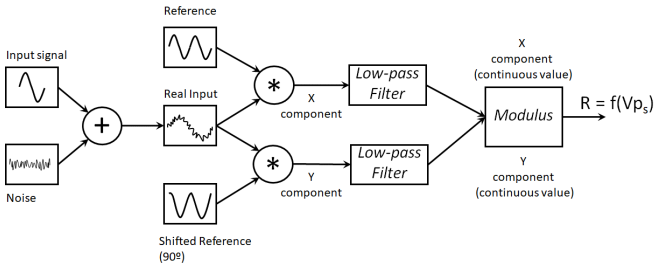

Fig. 4. LI amplification general scheme.

A. LI Technique

An LI can retrieve the amplitude and phase of an input signal using a reference signal at the same frequency. The typical two-phase implementation, which obtains the signal amplitude with independence of the phase difference between input and reference signal, consists of three steps: input and reference multiplication, low-pass filtering, and signal amplitude calculation.

The process, shown in Fig. 4, is executed in two branches: one with the reference signal with sine waveform and with the same frequency that the input signal and other with the 90° shifted reference. Assuming the input as a signal $V_{ps}\,\mathrm{sen}(\omega t)$ with a unique tone at f and a reference signal, $(\varphi V_{pr}\,\mathrm{sen}(\omega t+))$, the signal mix step is a multiplication that follows (1) and (2) for the first branch and (3) and (4) for the second branch. This mixing process provokes the shift and splitting of the signal centered on two new components: in dc and in $2f$ for this study case

$$X = V_s(t) * V_r(t) = V_{ps}\,\mathrm{sen}(\omega t) * V_{pr}\,\mathrm{sen}(\omega t + \varphi) \tag{1}$$

$$X = V_{ps}V_{pr}\left[\cos\varphi - \cos(2\omega t + \varphi)\right] \tag{2}$$

$$Y = V_s(t) * V_r\left(t + \frac{\pi}{2}\right) = V_{ps}V_{pr}\left[\mathrm{sen}(\omega t)\cdot\cos(\omega t + \varphi)\right] \tag{3}$$

$$Y = V_{ps}V_{pr}\left[\frac{\mathrm{sen}(2\omega t)}{2}\cos(\varphi) - \frac{(1-\cos(2\omega t))}{2}\,\mathrm{sen}(\varphi)\right]. \tag{4}$$

The next step is low-pass filtering, which produces the dc component of X and Y [see (5) and (6)], eliminating any non-dc component. Finally, the modulus calculation, using X and Y according to (7), produces a direct expression to obtain the peak voltage of input signal. Independently of the phase difference between both signals, the modulus calculation always gives the same result

$$X_{\mathrm{DC}} = \frac{1}{2}V_{ps}V_{pr}\cos\varphi \tag{5}$$

$$Y_{\mathrm{DC}} = \frac{1}{2}V_{ps}V_{pr}\sin\varphi \tag{6}$$

$$R = \sqrt{X^2 + Y^2} = \frac{V_{ps}V_{pr}}{2}. \tag{7}$$

The amplitude Vp is given by (8). Moreover, dual-phase LI allows to obtain the phase difference between the input and

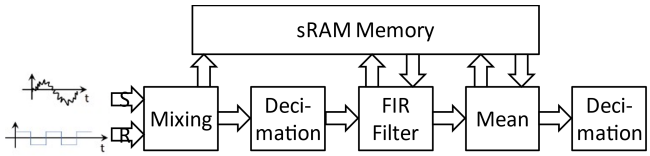

Fig. 5. Proposed digital LI architecture.

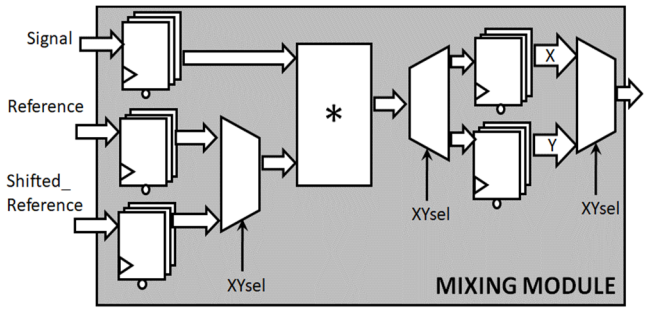

Fig. 6. Sine reference multiplication architecture.

reference signals with (9)

$$V_{ps} = \frac{2R}{V_{pr}} \tag{8}$$

$$\varphi = \tan^{-1}\left(\frac{Y_{\mathrm{DC}}}{X_{\mathrm{DC}}}\right). \tag{9}$$

B. Digital LI Design

As explained in Section I, the DS digital block must process data from four detectors (Pb/PbSe in forward/backward positions) with this LI architecture. The system operates at a clock frequency of 2 MHz, while the output rate has been selected as two data samples per second, guaranteeing a low data budget for uploading results to the CEU in the RDM instrument. As no hardware parallelization is possible, due to area restrictions, a time-multiplexed schedule has been designed (multipliers and temporary registers are shared through large multiplexers, controlled with the FSM). As the working frequency is much larger than the sampling frequency (2000 times), around 500 clock cycles are available for processing every sensed data of the four sensors timed multiplexed. We assure that data from each sensor are captured always at the same time instant and temporally stored in an external sRAM waiting for its turn. The proposed simple architecture is shown in Fig. 5, without detailing the multiplexers and demultiplexers at each processing block.

The digital architecture to obtain X and Y components is shown in Fig. 6. A 16-bit multiplier is required as ADC provides this word length for sensed digitized data. Registers required to store these values should be 32-bit wide if no truncation is performed. The more the truncation, the worse the precision would be in the results. Apart from bit truncation, the area restriction in aerospace instruments makes necessary additional hardware reduction. Hence, an optimized LI architecture is proposed, shown in Fig. 7, using a square reference signal instead of the sine one. The multiplier is substituted by a two-complement converter (CA2) for the input

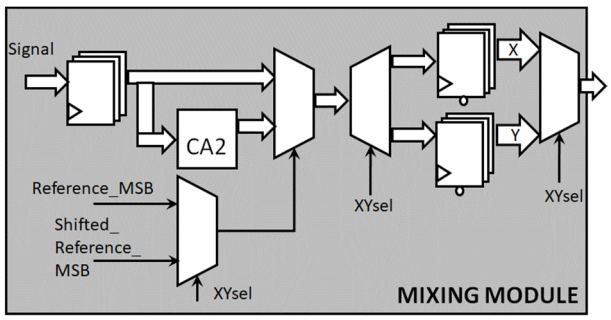

Fig. 7. Square reference multiplication architecture.

signal when required. The square reference signal ranges from -1 to 1 values. When this reference is -1, the input signal is CA2 converted, and when it is $+1$, the input signal is passed through directly.

However, this square reference signal provokes some inconveniences in the digital signal processing. In this case, X and Y components present secondary tones with comparable power to the fundamental one, and this can be seen in the Fourier series expansion of the square signal (10). The mathematical expression of X and Y components, using this reference, is detailed in (11) and (12), respectively. After low-pass filtering and modulus calculation, the peak voltage value is expressed in (13). Note that these low-pass filters should be more complex than in the case of sine reference, due to the appearance of a greater number of signal tones that must be removed

$$V_r(t) = \frac{4}{\pi} V_{pr} \cdot \sum_{n=1}^{\infty} \frac{1}{2n-1} \sin\left[(2n-1)\,\omega t + \varphi\right] \tag{10}$$

$$X = \frac{2}{\pi} V_{ps} V_{pr} \sum_{n=1}^{\infty} \frac{1}{2n-1} \times \left[\cos\left(2\,(1-n)\,\omega t - \varphi\right) - \cos\left(2n\omega t + \varphi\right)\right] \tag{11}$$

$$Y = \frac{2}{\pi} V_{ps} V_{pr} \sum_{n=1}^{\infty} \frac{1}{2n-1} \times \left[\sin\left(2n\omega t + \varphi\right) - \sin\left(2\,(1-n)\,\omega t - \varphi\right)\right] \tag{12}$$

$$R = \frac{2 \cdot V_{ps} V_{pr}}{\pi} \rightarrow V_{ps} = \frac{\pi \cdot R}{2 \cdot V_{pr}} \tag{13}$$

The IR emitter modulation frequency is fixed at 10 Hz, and the detectors' analog signals are digitalized by an ADC at a sampling frequency of 1 ksps ($fs = 100f$) that guarantees a high resolution. After multiplication, the sampling frequency is reduced to $fs = 20f$ in the decimation step. As a high restrictive low-pass filter (LPF) requires too many resources to be implemented in this system, two processes optimized in resources are used to eliminate the harmonics generated in the multiplication and reduced the noise at other frequencies. A detailed scheme of this architecture is shown in Fig. 8.

The two processes implemented split the filtering requirements to reduce the number of resources needed. First, a light low-pass FIR filter (five taps) was obtained with the MATLAB[1] "*filterDesigner*" tool. This filter was specifically designed for signals obtained from a square reference

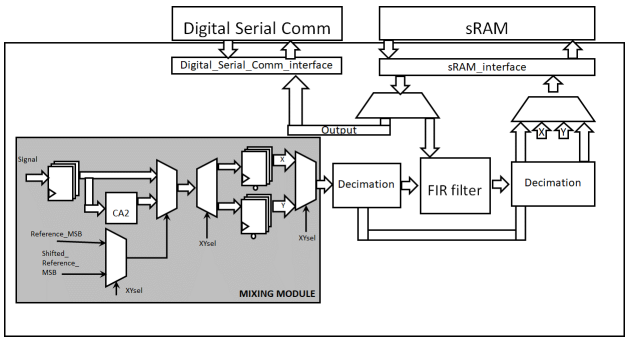

Fig. 8. Digital LI architecture.

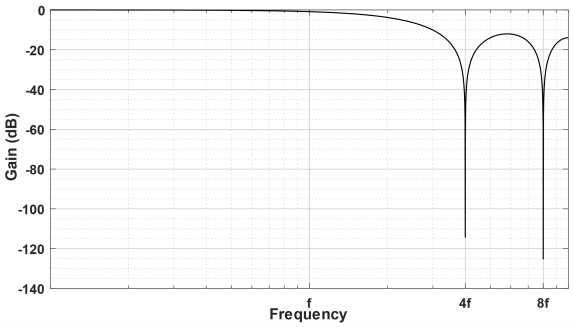

Fig. 9. FIR filter frequency response.

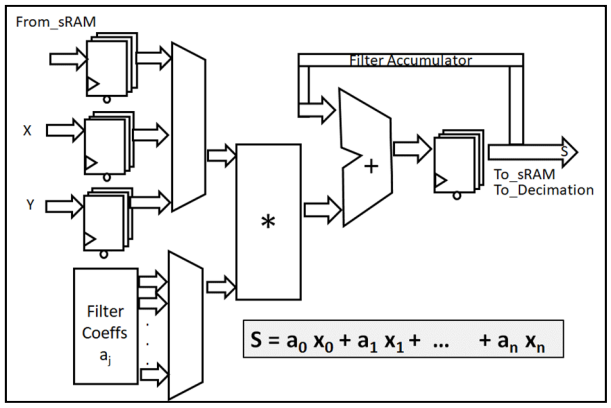

Fig. 10. FIR filter serial architecture.

[see (11) and (12)] and presents two notches at $0.2fs$ and $0.4fs$. With an fs/f ratio of 20, these notches will filter $4f$ and $8f$ (Fig. 9). This filter is implemented in a serial architecture, as shown in Fig. 10. Second, the response of this filter was completed with the next step, a mean of four samples. This process calculates the mean value of four equidistant samples in a single period, eliminating all harmonics integer multiples of f, except the 4th and 8th ones (Fig. 11). The result of this process is the dc component of X and Y. Furthermore, it was verified through the tests that the error was minimized with the use of 8 bits in the FIR coefficients, which implied fewer resources required for multipliers and adders.

The last step is a second decimation process that downsamples to $fs = 2$ Hz to guarantee the data rate requirement, 2 samples/s. The output of this system contains the X_{DC} and

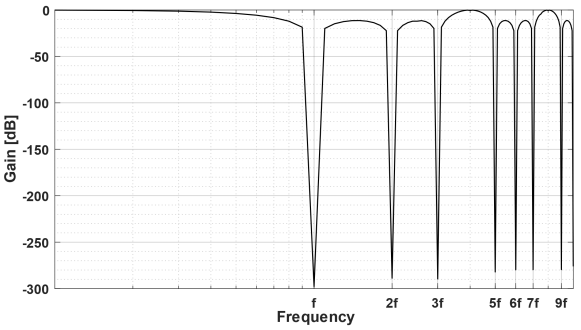

Fig. 11. Mean frequency response.

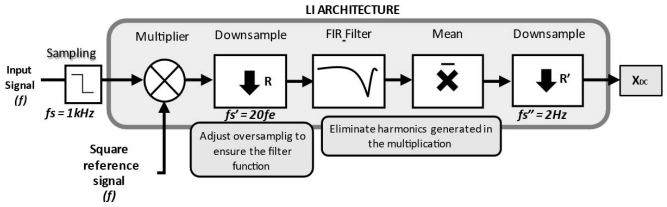

Fig. 12. Adaptable LI architecture.

Y_{DC} components. The final calculation of Vp, and the phase if required, will be executed once data were received at Earth.

Due to oversampling and decimation step, this LI architecture is easily adaptable to multiple frequencies for the input signal. By changing the downsampling ratio to guarantee $fs = 20f$ in the FIR filter and mean steps, the harmonics at frequencies integer multiples of f will always be eliminated. This adaptable LI architecture, shown in Fig. 12, allows the system to work with IR source excitement signals at different frequencies.

Through digital serial communication, it is possible to reconfigure the DS to work with a different excitement frequency f, while the system is running. In this case, the system generates the excitement reference signals at the new frequency f and selects the decimation ratios (R for the first decimation step and R' for the second decimation step, see (14) and (15), respectively) to adapt the LI at f

$$R = \frac{fs}{20f} \tag{14}$$

$$R' = \frac{20f}{2}. \tag{15}$$

IV. Results

This section presents the experimental results obtained with the DS system. The tests were performed with a DS calibration model (CM), whose design, architecture, and functionality are those presented in the previous sections while implemented with commercial components. In this CM, the digital circuit has been implemented in an FPGA Microsemi ProAsic 3 plus an SRAM module (1 Mbit). The DS-CM is shown in Fig. 13.

A. Error Characterization

In order to see how the system behaves with regard to the SNR parameter. A campaign of tests was performed to

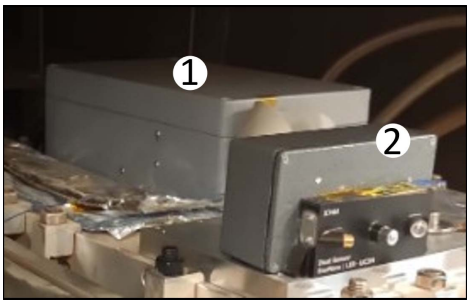

Fig. 13. DS-CM during an experiment. 1: digital LI and power supply. 2: analog front-end and IR devices.

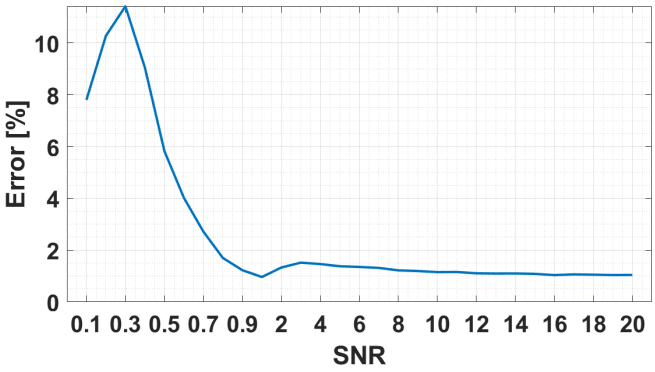

Fig. 14. Graph of output error versus SNR of input signals with amplitude 1 V.

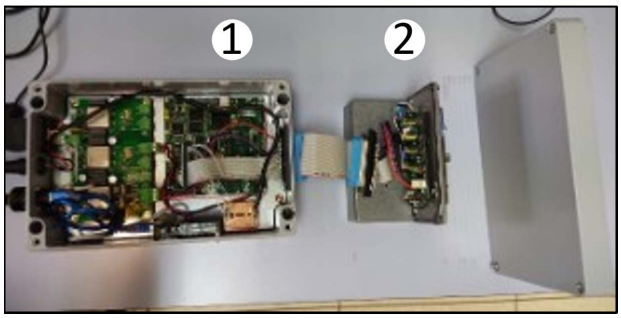

Fig. 15. Experiment setup. 1: digital LI and power supply. 2: analog front-end and IR devices.

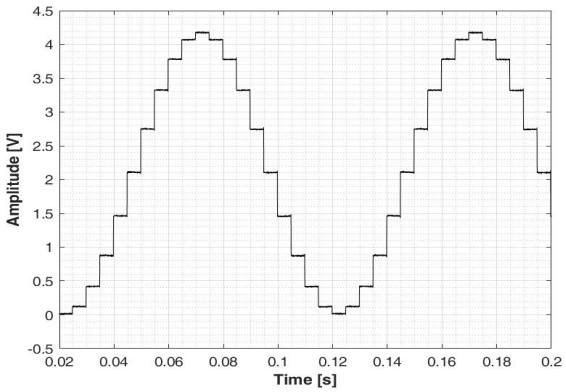

Fig. 16. DAC output obtained by oscilloscope.

measure the relative error between Vp of the input signal and the data obtained from the digital LI implemented. The results are shown in Fig. 14.

For this test, a sine-wave signal of 1-V amplitude was created in MATLAB and fouled with noise according to the SNR chosen in each iteration. The noise employed is representative of a Gaussian white noise with normal distribution. This signal has been processed in the digital LI implemented and Vp has been obtained according to (13) and compared with respect to the input value, 1 V at 10 Hz. The same seed has been used for noise generation in every point of the curve, increasing the noise power distribution to reduce SNR. The relative error has been calculated according to the following equation:

$$E\,[\%] = \frac{|Va - Vo|}{Va} * 100 \tag{16}$$

where *Va* is the peak voltage of the generated signal without error and *Vo* is the peak voltage obtained by the digital LI processing of *Va* signal plus noise.

Analyzing the relative error represented in Fig. 14, the values obtained for SNR higher than 0.8 are less than 1.8%, even 1% for SNR higher than 8. On the other hand, the relative error is much higher with lower SNRs, reaching 12% for SNR equal to 0.3. This fact is due to the limited precision of the digital system.

We can conclude that when the levels of noise are doubling the input signal Vp, the relative error in the output is between 6% and 12%; but, on the contrary, for lower levels of noise, the relative error is below 1%, better than the results reported in the literature [38].

B. Experimental Testing

To analyze the data during the operation of the implemented system, Fig. 15, test points were introduced on the analog circuit to observe signals between functional blocks. For this purpose, the RIGOL DS4014E digital oscilloscope and the proprietary software tool UltraScope in version 00.01.02.12 and Ultra Sigma in version 00.01.06.01 were used. With the help of these tools, analog signal values were captured at test points during the test campaigns. These signals were digitally recorded for analysis with a high resolution of 500 kSps for a time window of 14 s. MATLAB software tool R2020b was used for sampling, processing, and analysis of the captured signals.

During testing, the signal output of the DAC (Figs. 2 and 3), which is used in the excitation of the IR emitter source, was checked. This signal is generated in the DS digital circuit to serve as an input to the DAC. The generated signal corresponds to a 10-Hz sine and peak-to-peak amplitude of 4.2 Vpp (peak-to-peak voltage) generated with discretization steps due to the resolution and scale background of the DAC. The signal obtained is shown in Fig. 16. The subsequent filter is applied to this signal before modulating the IR emitter.

To test the response of the two types of sensors present in the instrument, a test scheme was designed using a flat solid metallic object of gray color (#BEBAB7). This object was placed at certain distances from the outer edge of the sensors in the "backward" position, facing parallel to each other between surfaces. These distances were selected so that the PbS and PbSe composition sensors would provide a readily appreciable

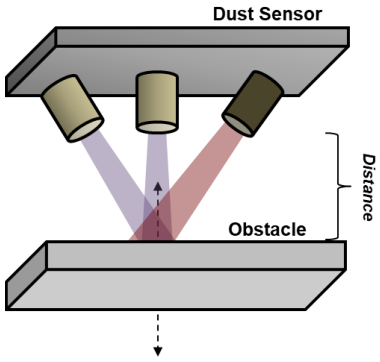

Fig. 17. Experiment schematic.

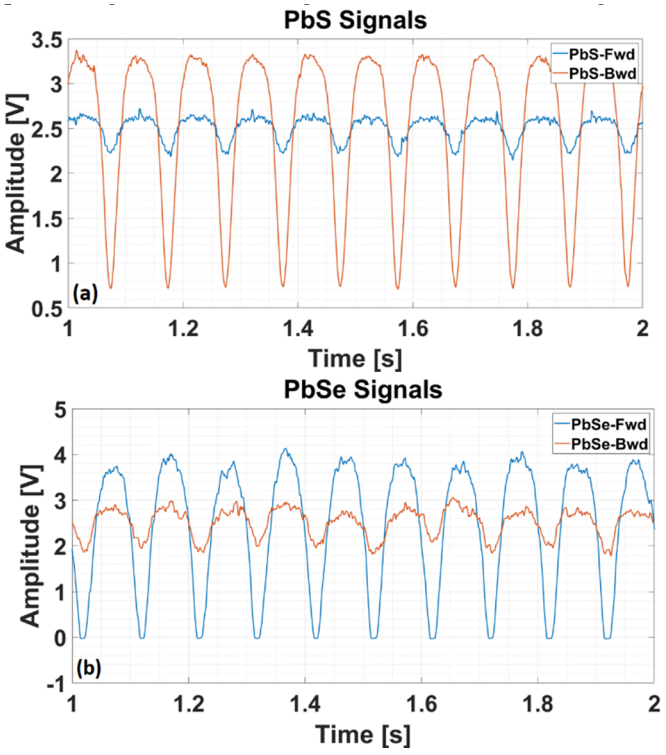

Fig. 18. Response of (a) PbS and (b) PbSe detectors for experimental setup, Fig. 17, with distances of 7.5 cm (a) and 2.9 cm (b).

and unsaturated response for their respective distance from the obstacle. A schematic of the experiment setup is shown in Fig. 17.

The signals shown in Fig. 18 are in the time domain in correspondence with the response of the detectors at the output of analog amplification step. The PbS detectors' signals correspond to a distance between object and instrument of 7.5 cm, and the PbSe signals correspond to a separation of 2.9 cm. These signals present a periodic waveform, not exactly sine-shaped due to the presence of lower amplitude frequency components in tones different from the carrier of the generated excitation signal. This effect is due to the power response of the emitter when excited, modulating the signal, and to the coupling of signals in the form of noise to a lesser extent. The frequency tones of each signal shown can be seen in Fig. 19.

In Fig. 19, these same signals (PbS detectors' signal with 7.5 cm and PbSe detectors' signal with 2.9 cm as distances

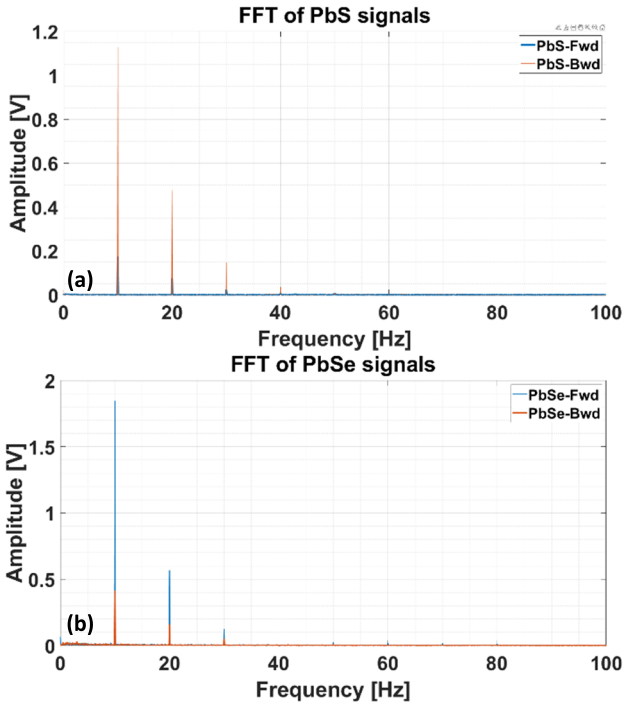

Fig. 19. Frequency response of (a) PbS at 7.5 cm of distance and (b) PbSe at 2.9 cm of distance detectors.

between object and instrument) are shown in the frequency domain, to obtain the main tones of the frequency spectrum. The main component is appreciated with the highest power contribution at 10 Hz and harmonics at 20 and 30 Hz with decreasing amplitude. The signals originally have a dc component, with an approximate value of 2.5 V, which is extracted before performing the fast Fourier transform in order to observe the signal in the frequency domain. Once the signal is received, the processing of the signal will focus on the frequency of interest (10 Hz) and the harmonics that can interfere with the process, so the dc component is eliminated.

The presence of harmonics in the signal, which may exist due to average and nonideal components, will affect the final result. These unwanted harmonics will be attenuated by the analog electronics and, then, almost entirely eliminated by the digital LI in the FPGA. If there are unwanted harmonics at multiple odd frequencies of f, the mixing process with a square reference signal will generate components at 0 Hz, as described in (10) and (11). These unwanted dc components will be added to the signal of interest, directly affecting the final voltage result and increasing its error. All the above contribute to a difference between the expected value and the obtained result, interpreted as an error, which is added to the error provoked by the digital implementation, and the signal processing resolution. The global error is shown in Fig. 20.

Fig. 20 shows the calculated Vp, obtained with the captured signals at the output of analog amplification step and Vp delivered by the LI for each sensor. The graphs shown correspond to four samples referring to the mean calculated Vp and Vp for 10-Hz tone per campaign. The difference between both lines in relation to the expected Vp is the error shown

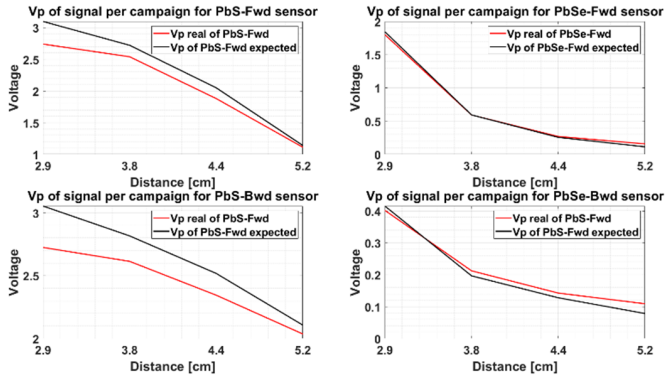

Fig. 20. Vp registered and calculated for each sensor.

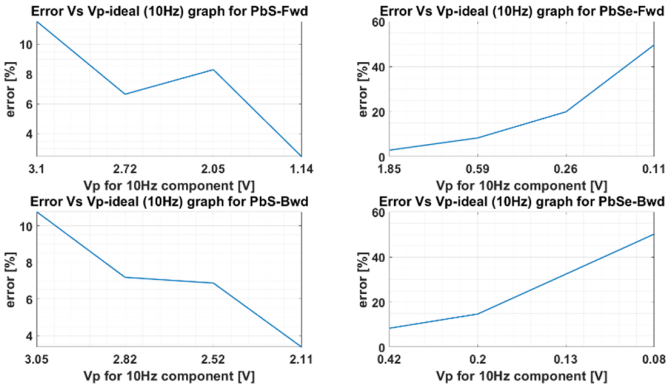

Fig. 21. Error graph with regard to calculated Vp for each sensor.

in Fig. 21. The image shows four plots referring to every sensor, PbS forward, PbSe forward, PbS backward, and PbSe backward. These graphs are based on the error rate against the expected Vp in the 10-Hz component, which is ordered downward. Depending on the obstacle, with the decrease of Vp of signal captured, the trend in the PbS-type sensors is the decrease of the error, while the opposite case is observed in PbSe. This effect is observed for small ideal Vp levels, so the difference between calculated and real Vp values will be more significant by increasing the percentage error. On the other hand, the error for small signals is defined by the resolution reached by the LI digitally implemented. Due to resource and area constraints, data are truncated losing resolution in the result.

The maximum resolution for the system under study is determined by the accuracy of the ADC, with 5-V full scale and 16 bits, and the Vlsb calculation is shown in (17). Added to it, the data processing in the system leads to an increase of bits, so it is necessary to truncate the eight least significant bits, degrading the overall system resolution, as shown in (18), to 0.0195 V approximately. For the reasons stated above, for low detected signal levels, the error will increase significantly. In the experiments, it was found that the PbSe detectors deliver a small-signal response relative to the PbS, which is why the error tends to be larger, as shown in Fig. 21. The final implementation after resource optimization required the

TABLE I
PERCENT OF THE UTILIZATION OF FPGA RESOURCES

	Target Part: 54sx32a-2		
	Available	Used	Occupation [%]
Sequential	1,080	651	60.28
Combinational	1,800	1,690	93.89
Logic (Seq+Comb)	2,880	2,341	**81.28**
IO w/ Clocks	81	48	

TABLE II
SYSTEM CONSUMPTION

State	Current consumption per line [mA]		
	5V line	+12V line	-12V line
Idle	46	5	4
Warm-Up	47	134	4
Sensing	47	141	4
Telemetry	70	5	4

occupancy described in Table I

$$V_{\mathrm{LSB}} = \frac{5}{2^{16} - 1} \tag{17}$$

$$\text{Resolution} = 2^8 \cdot V_{\mathrm{LSB}} \cong 0.0195 \text{ V}. \tag{18}$$

As it can be seen, the total occupation between combinational and sequential logic circuits is 81.28%. It can be concluded that very efficient use of resources and area was achieved. On the other hand, the current consumption reached by the flight model (FM), measured at INTA facilities, is shown in Table II.

Consumption levels per line are minimum in the "Idle" state and reach maximum levels in "Warm-Up" and "Sensing" due to the activation of the emitter and the operation of the ADC and LI. In the case of the "Telemetry" status, the measurement system will be inactive, but this is not the case with the communication block, powered by the 5-V line, which will be exchanging data. As can be seen, the current consumption is very small and consistent between all its states.

V. CONCLUSION

This article proposes an optimized digital architecture design for signal processing of DS, a multisensor dust detection instrument designed by the Universidad Carlos III de Madrid (Spain) and manufactured at INTA facilities. This instrument is part of EXOMARS mission, which would investigate the possible signs of life on Mars and explore its environment.

The data provided by DS will serve to retrieve the local distribution of dust particles suspended in Mars' surface by scattering caused by the particles on an IR beam. To process the signals detected by its four IR sensors, a digital LI has been implemented in a rad-hard Microsemi[1] FPGA (RT54SX32S), with all its flip-flops triplicated and a rad-hard 1 MB sRAM

memory (256 k × 32). The working frequency is 2 MHz and with a high occupation of the available area.

In the article, the DS system and its components have been presented to show the advantages of the optimized digital architecture and the digital signal processing proposed. An area-optimized digital LI is proposed for this architecture. The described architecture saves resources by using a square signal reference and filters with very low steps, allowing to process the four signals in real time using a single LI. This is possible by reusing resources and storing partial results in an external 1-Mb SRAM. In the FPGA, 81.28% of the available components have been used. The current consumption is very low: 70 mA (5 Vdc) during telemetry (4.3 s/h) and 134–141 mA (12 Vdc) during measurement (5 + 10 min/h).

Furthermore, this architecture allows flexibility and processing capacity, achieving a data budget with a high rate of processed versus sent data and meeting the requirements for a planetary exploration system. On the other hand, experimental tests have been performed to see the system accuracy and power consumption. Although the EXOMARS mission has been suspended,[2] the instrument and all the results and knowledge gained are documented and can serve as a basis for future research and aerospace missions.

Acknowledgment

The authors wish to acknowledge the huge help provided by the personnel at the National Institute of Aerospace Techniques: Javier Martínez Oter, Felipe Serrano Santos, Javier Manzano Vázquez, Ignacio Arruego Rodríguez, and the rest of the people at the Payloads and Space Sciences Department.

References

[1] E. Stuhlinger, "Sputnik 1957-memories of an old timer," *J. Brit. Interplanetary Soc.*, vol. 52, pp. 235–238, Oct. 1997.

[2] J. Ellis, "Brains unlimited: Giftedness and gifted education in Canada before Sputnik (1957)," *Can. J. Educ./Revue Canadienne De L'Éducation*, vol. 40, no. 2, pp. 1–26, 2017.

[3] R. Uzel and A. Ozyildirim, "A study on the local shielding protection of electronic components in space radiation environment," in *Proc. 8th Int. Conf. Recent Adv. Space Technol. (RAST)*, Jun. 2017, pp. 295–299, doi: 10.1109/RAST.2017.8003007.

[4] M. Boscherini et al., "Radiation damage of electronic components in space environment," *Nucl. Instrum. Methods Phys. Res. A, Accel. Spectrom. Detect. Assoc. Equip.*, vol. 514, no. 1, pp. 112–116, 2003. Available:, doi: https://doi.org/10.1016/j.nima.2003.08.091.

[5] X. J. Jiang et al., "Suitability analysis of commercial off-the-shelf components for space application," *Proc. Inst. Mech. Eng., G, J. Aerosp. Eng.*, vol. 220, no. 5, pp. 357–364, 2006.

[6] NASA. *Mars 2020 Perseverance Rover*. Accessed: Oct. 19, 2022. [Online]. Available: https://mars.nasa.gov/mars2020/

[7] *ExoMars*. Accessed: Oct. 19, 2022. [Online]. Available: https://www.esa.int/Science_Exploration/Human_and_Robotic_Exploration/Exploration/ExoMars

[8] D. W. Davies, "Effects of dust on the heating of Mars' Surface and atmosphere," *J. Geophys. Res.*, vol. 84, pp. 8289–8293, Dec. 1979, doi: 10.1029/JB084iB14p08289.

[9] G. A. Landis, "Mars dust-removal technology," *J. Propuls. Power*, vol. 14, no. 1, pp. 126–128, Jan. 1998, doi: 10.2514/2.5258.

[10] R. T. Clancy and S. W. Lee, "A new look at dust and clouds in the Mars atmosphere: Analysis of emission-phase-function sequences from global viking IRTM observations," *Icarus*, vol. 93, no. 1, pp. 135–158, 1991, doi: https://doi.org/10.1016/0019-1035(91)90169-T.

[11] R. T. Clancy et al., "An intercomparison of ground-based millimeter, MGS TES, and Viking atmospheric temperature measurements: Seasonal and interannual variability of temperatures and dust loading in the global Mars atmosphere," *J. Geophys. Res.*, vol. 105, pp. 9553–9571, 2000, doi: https://doi.org/10.1029/1999JE001089.

[12] *Mars Pathfinder Science Results*. Accessed: Oct. 19th, 2022. [Online]. Available: https://mars.nasa.gov/MPF/science/atmospheric.html

[13] A. Russu et al., "A light compact and rugged IR sensor for space applications," *Proc. SPIE*, vol. 11129, pp. 57–64, Sep. 2019.

[14] H.-H. Highsmith, J. E. Brock, and D. E. Stephens, "Space launch system (SLS) data acquisition and sensor system for human space flight," in *Proc. IEEE Aerosp. Conf.*, Mar. 2015, pp. 1–9, doi: 10.1109/AERO.2015.7119024.

[15] J. Pérez-Izquierdo et al., "The thermal infrared sensor (TIRS) of the Mars environmental dynamics analyzer (MEDA) instrument onboard Mars 2020," in *Proc. IEEE Int. Workshop Metrology Aerosp. (MetroAeroSpace)*, Jun. 2017, pp. 79–84, doi: 10.1109/MetroAeroSpace.2017.7999542.

[16] M. Yim, K. Roufas, D. Duff, Y. Zhang, C. Eldershaw, and S. Homans, "Modular reconfigurable robots in space applications," *Auto. Robots*, vol. 14, no. 2, pp. 225–237, Mar. 2003, doi: 10.1023/A:1022287820808.

[17] S. P. Rawal, "Metal-matrix composites for space applications," *JOM*, vol. 53, no. 4, pp. 14–17, Apr. 2001, doi: 10.1007/s11837-001-0139-z.

[18] H. Guzman-Miranda, M. A. Aguirre, and J. Tombs, "A non-invasive system for the measurement of the robustness of microprocessor-type architectures against radiation-induced soft errors," in *Proc. IEEE Instrum. Meas. Technol. Conf.*, May 2008, pp. 2009–2014, doi: 10.1109/IMTC.2008.4547378.

[19] F. Siegle, T. Vladimirova, J. Ilstad, and O. Emam, "Mitigation of radiation effects in SRAM-based FPGAs for space applications," *ACM Comput. Surv.*, vol. 47, no. 2, pp. 1–34, Jan. 2015, doi: 10.1145/2671181.

[20] X. Qun and Z. Jian, "Improved SNR estimation algorithm," in *Proc. Int. Conf. Comput. Syst., Electron. Control (ICCSEC)*, Dec. 2017, pp. 1458–1461, doi: 10.1109/ICCSEC.2017.8446894.

[21] R. O. S. Juan, B. H. Ko, C. S. Park, and H. S. Kim, "Development of a reduction algorithm for CAN frame bits," in *Proc. Int. SoC Design Conf. (ISOCC)*, Nov. 2017, pp. 127–128, doi: 10.1109/ISOCC.2017.8368802.

[22] L. A. Garcia-Astudillo, L. Entrena, A. Lindoso, H. Martin, P. Martin-Holgado, and M. Garcia-Valderas, "Analyzing reduced precision triple modular redundancy under proton irradiation," *IEEE Trans. Nucl. Sci.*, vol. 69, no. 3, pp. 470–477, Mar. 2022, doi: 10.1109/TNS.2022.3152088.

[23] D. Brooks, "Differential signals," CMP Media Publication, Tech. Rep., Oct. 2001. Accessed: Oct. 19, 2022. [Online]. Available: https://www.ieee.li/pdf/essay/differential_signals.pdf

[24] W.-T. Liu, C.-H. Tsai, T.-W. Han, and T.-L. Wu, "An embedded common-mode suppression filter for GHz differential signals using periodic defected ground plane," *IEEE Microw. Wireless Compon. Lett.*, vol. 18, no. 4, pp. 248–250, Apr. 2008, doi: 10.1109/LMWC.2008.918883.

[25] C.-Y. Chang and D.-R. Chen, "Active noise cancellation without secondary path identification by using an adaptive genetic algorithm," *IEEE Trans. Instrum. Meas.*, vol. 59, no. 9, pp. 2315–2327, Sep. 2010.

[26] H. H. Asada, H.-H. Jiang, and P. Gibbs, "Active noise cancellation using MEMS accelerometers for motion-tolerant wearable bio-sensors," in *Proc. 26th Annu. Int. Conf. IEEE Eng. Med. Biol. Soc.*, Sep. 2004, pp. 2157–2160, doi: 10.1109/IEMBS.2004.1403631.

[27] C. Stagner, A. Conrad, C. Osterwise, D. G. Beetner, and S. Grant, "A practical superheterodyne-receiver detector using stimulated emissions," *IEEE Trans. Instrum. Meas.*, vol. 60, no. 4, pp. 1461–1468, Apr. 2011, doi: 10.1109/TIM.2010.2101330.

[28] M. Tohidian, I. Madadi, and R. B. Staszewski, "A fully integrated discrete-time superheterodyne receiver," *IEEE Trans. Very Large Scale Integr. (VLSI) Syst.*, vol. 25, no. 2, pp. 635–647, Feb. 2017, doi: 10.1109/TVLSI.2016.2598857.

[29] R. W. Budding and L. Strackee, "A simple reference generator for lock-in amplifiers," *J. Phys. E, Sci. Instrum.*, vol. 5, no. 8, p. 744, 1972.

[30] D. P. Blair and P. H. Sydenham, "Phase sensitive detection as a means to recover signals buried in noise," *J. Phys. E, Sci. Instrum.*, vol. 8, no. 8, p. 621, 1975.

[31] M. L. Meade, "Advances in lock-in amplifiers," *J. Phys. E, Sci. Instrum.*, vol. 15, no. 4, p. 395, 1982.

[32] K. Kishore and S. A. Akbar, "Evolution of lock-in amplifier as portable sensor interface platform: A review," *IEEE Sensors J.*, vol. 20, no. 18, pp. 10345–10354, Sep. 2020, doi: 10.1109/JSEN.2020.2993309.

[2] https://www.esa.int/Newsroom/Press_Releases/ExoMars_suspended

[33] F. Barone, E. Calloni, L. Di Fiore, A. Grado, L. Milano, and G. Russo, "High-performance modular digital lock-in amplifier," *Rev. Sci. Instrum.*, vol. 66, no. 6, pp. 3697–3702, Jun. 1995.
[34] J. M. Masciotti, J. M. Lasker, and A. H. Hielscher, "Digital lock-in detection for discriminating multiple modulation frequencies with high accuracy and computational efficiency," *IEEE Trans. Instrum. Meas.*, vol. 57, no. 1, pp. 182–189, Jan. 2007.
[35] S. Ma, J. Schroder, and P. Hauptmann, "Sensor impedance spectrum measurement interface with lock-in amplifier," in *Proc. IEEE SENSORS*, Jun. 2002, pp. 1313–1316.
[36] J. Lu, D.-A. Pan, B. Yang, and L. Qiao, "Wideband magnetoelectric measurement system with the application of a virtual multi-channel lock-in amplifier," *Meas. Sci. Technol.*, vol. 19, no. 4, Apr. 2008, Art. no. 045702.
[37] M. O. Sonnaillon and F. J. Bonetto, "A low-cost, high-performance, digital signal processor-based lock-in amplifier capable of measuring multiple frequency sweeps simultaneously," *Rev. Sci. Instrum.*, vol. 76, no. 2, Feb. 2005, Art. no. 024703.
[38] W. B. Larbi et al., "Experimental comparison of lock-in and pulsed thermography for the nondestructive evaluation of aerospace materials," in *Proc. 6th Int. Workshop-NDT Signal Process. (ASPNDE)*, London, ON, Canada, Aug. 2009.
[39] C. Zhang, H. Liu, J. Ge, and H. Dong, "FPGA-based digital lock-in amplifier with high-precision automatic frequency tracking," *IEEE Access*, vol. 8, pp. 123114–123122, 2020, doi: 10.1109/ACCESS.2020.3006070.
[40] L. Colangeli et al., "The Giada experiment for the Rosetta mission," in *The New Rosetta Targets*, vol. 311. Dordrecht, The Netherlands: Springer, 2004, doi: 10.1007/978-1-4020-2573-0_25.
[41] P. Palumbo et al., "The MAGO experiment for dust environment monitoring on the Martian surface," *Adv. Space Res.*, vol. 33, no. 12, p. 2252, 2004, doi: 10.1016/s0273-1177(03)00517-9.
[42] L. Colangeli et al., "MEDUSA: The ExoMars experiment for in-situ monitoring of dust and water vapour," *Planet. Space Sci.*, vol. 57, no. 8, pp. 1043–1049, 2009, doi: 10.1016/j.pss.2008.07.013.
[43] F. Esposito et al., "MEDUSA: Observation of atmospheric dust and water vapor close to the surface of Mars," *Citation, Mars*, vol. 6, p. 1, Jun. 2011, doi: 10.1555/mars.2011.0001.
[44] D. Scaccabarozzi et al., "MicroMED, design of a particle analyzer for Mars," *Meas., J. Int. Meas. Confederation*, vol. 122, pp. 466–472, Jul. 2018, doi: 10.1016/j.measurement.2017.12.041.
[45] D. Scaccabarozzi et al., "MicroMED optical particle counter: From design to flight model," *Sensors*, vol. 20, no. 3, p. 611, 2020, doi: 10.3390/s20030611.

Alberto Ramírez Bárcenas received the bachelor's degree in industrial electronics and automation engineering and the M.Sc. degree in electronic systems and applications engineering from the Universidad Carlos III de Madrid, Madrid, Spain, in 2018 and 2019, respectively, where he is pursuing the Ph.D. degree in industrial electronics program.

His research field comprises fault-tolerant design, online testing, and hardware/software codesign. He has been a part of the DS-EXOMARS20 Exploration Project at the Universidad Carlos III de Madrid, participating in the development of the dust sensor, an instrument that aimed to measure the dust present on the surface of Mars. Moreover, he is a part of UC3M4Safety, a multidisciplinary team that proposes to use technology to protect women at risk of sexual- or gender-based violence.

Rolando Paz Herrera graduated in electronics and telecommunications engineering from the Central University "Marta Abreu" of Las Villas (UCLV), Santa Clara, Cuba, in 2016, and received the master's degree in electronic systems engineering and applications from the Universidad Carlos III de Madrid, Madrid, Spain, in 2020.

From February 2021 to October 2022, he was a part of the multidisciplinary European project Exomars'20 (extended to in Mars) focused on the development of the sensor dust system for dust measurements on the surface of Mars.

Jose A. Miranda Calero (Member, IEEE) received the B.Sc. degree in industrial electronics and automation engineering, the M.Sc. (Hons.) degree in electronic systems and applications engineering, and the Ph.D. (Hons.) degree from the Universidad Carlos III de Madrid, Madrid, Spain, in 2012, 2015, and 2022, respectively.

From 2012 to 2015, he worked as an embedded software engineer in different countries within Europe for public and private sectors. He is currently a Postdoctoral Researcher at the École polytechnique fédérale de Lausanne (EPFL) School, Lausanne, Switzerland. His research field comprises a wireless sensor network, wearable design, development and integration for safety applications, affective computing implementation into edge computing devices, and hardware acceleration. He is also a part of UC3M4Safety, a multidisciplinary team that proposes to use technology to protect women at risk of sexual- or gender-based violence. Regarding hardware acceleration of digital signal processing from sensors, he has also participated in other projects related to space applications, such as DS-EXOMARS20.

Manuel F. Canabal graduated in industrial technologies engineering and received the master's degree in electronic systems and applications engineering from the Universidad Carlos III de Madrid (UC3M), Madrid, Spain, in 2015 and 2017, respectively.

From 2017 to 2022, he has worked as a Graduate Engineer with the Electronic Technology Department of UC3M in different research fields, such as mixed-signal microelectronics, space instruments, affective computing, and the integration of this technology in edge devices. He is a part of the UC3M4Safety team that aims to provide a technological solution to combat gender violence from a multidisciplinary perspective. Moreover, he has made research on the use of new biosensors to improve Bindi's capabilities and functionality. Regarding smart sensor design, he has also participated in other projects related to space applications, such as DS-EXOMARS20.

Ernesto García Ares graduated in telecommunication engineering from the Universidad Politécnica de Madrid, Madrid, Spain, in 1994.

From October 1994 to February 1999, he was a Teaching Assistant with the Electronics Technology Department, Universidad Carlos III de Madrid, Madrid. He then worked as a Project Manager at T.G.I: SA, Madrid, from February 1999 to July 2000 and Grupo Interlab SA and Interlab IEC SA, Madrid, from July 2000 to June 2005, and the Head of the non destructive testing (NDT) Department, Interlab IEC SA, from June 2005 to May 2007, where he worked in the conception and design of ultrasonic NDT automated systems. Since May 2007, he has been the Head of the Electronics Design Office, Universidad Carlos III de Madrid. Throughout his professional life, he has worked as a design engineer of application-specific analog circuits, including sensor signal conditioning, low noise, high bandwidth front ends, hi-rel designs for aerospace applications, hardware-in-the-loop testbeds for renewable power generation plants, and power management systems for energy poverty applications.

Andres Russu is an Aerospace Engineer with a large experience in space science instrumentation development. The experience with payloads on different wavelengths is from radio up to cosmic rays and Sun energetic particles. He has been working as a project manager in Exomars dust sensor with the Infrared Laboratory, Physics Department, Universidad Carlos III de Madrid, Madrid, Spain.

Francisco Cortés received the Ph.D. degree in industrial engineering with "contribution to the solution of the reverse problem in the remote detection of gases and particles by spectral radiometry and infrared imaging" from the Universidad Carlos III de Madrid (UC3M), Madrid, Spain, in 2016.

He is currently the CEO of the spin-off company Sensia Solutions, Leganés, Madrid, created in 2105 and with a great activity in the IR technology with diverse industrial and technological applications.

Antonio J. de Castro received the Ph.D. degree in physics of condensed matter from the Universidad Complutense de Madrid, Madrid, Spain, in 1992.

He was a member of the International Consortium—Japanese Experiment Module-Extreme Universe Space Observatory. He has an extensive experience in international research and development space projects. His domains of experience and expertise are related to the use of Fourier transform infrared spectroradiometry and spectrophotometry focused on the remote sensing of forest fires, combustion monitoring, control of pollutant gases in the atmosphere, and the measurement of physical properties of clouds. He is also involved in the modeling of the infrared scenarios associated with these problems in order to develop methodologies to retrieve the physical information under interest. He is currently an Associate Professor with the Department of Physics, Universidad Carlos III de Madrid, Madrid. He has been a part of the UC3M Team and the METNET Mission. He also holds the scientific responsible for instrument dust Sensor (DS) to be launched on the next ExoMars Mission. He is devoted to the measurement of physical properties of the suspended dust at the surface of Mars.

Fernando López received the Ph.D. degree in physics from the Universidad Complutense de Madrid, Madrid, Spain, in 1988.

He is a Professor at the Department of Physics, Universidad Carlos III de Madrid (UC3M), Madrid. His lines of research focus on the study of the interaction infrared radiation (IR)—matter and its applications to gas sensors and properties of solids, remote sensing, IR thermography, multispectral and hyperspectral imaging, and aerospace and optical applications in general. He has supervised seven doctoral theses and has published around 100 scientific articles, 70 in the Science Citation Index (Web of Science). Average citations received over the past five years: 27 appointments per year (300 total). He has been the PI in 27 research and development projects in competitive, national, and international public calls (six European projects) and in more than 60 research contracts with administrations and companies. He is the Founder and the Head of the LIR-Infrared Laboratory, a research group at the UC3M that has contributed to the training in advanced IR optics of more than 60 young physicists and engineers, through scholarships and research contracts. It has the most important endowment in IR imaging systems of the Spanish university, which allows it to participate in large research projects, including space missions. He is a Promoter of “spin-off” of the UC3M for the transfer to industry and society of the scientific capabilities of the LIR in IR sensor technology (Sensia Solutions).

Dr. López Martínez was a recipient of the Medal of Naval Merit.

Marta Portela-García received the Ph.D. degree in electronic engineering from the University Carlos III of Madrid, Madrid, Spain, in 2007.

She is an Assistant Professor with the Electronic Technology Department, Universidad Carlos III de Madrid, Madrid, and currently working as a Senior Researcher at the Arquimea Research Center, Canary Islands, Spain. Her current research interests include embedded systems, hardware acceleration, FPGA-based systems, and very large-scale integration digital design.

Celia Lopez-Ongil (Senior Member, IEEE) received the M.Sc. degree in industrial engineering and the Ph.D. degree in digital techniques from the Universidad Politécnica de Madrid, Madrid, Spain, in 1995 and 2000, respectively.

In 1998, she joined the Universidad Carlos III of Madrid, Madrid, as an Assistant Professor. Since 2010, she has been an Associate Professor at the Department of Electronic Technology. Her research was framed in the line of robust circuits for space applications in the first 20 years, focused on the generation of HW/SW tools to ensure the quality and reliability of microelectronic circuits, and produced two Ph.D. theses, 19 articles in scientific journals, and 90 contributions at international conferences. Some designs in space missions (ASCAT-METOP, SADE-ROSETTA, and DS-EXOMARS20) can be highlighted. Since 2016, her research has focused on cyber-physical systems, dedicated to detecting, preventing, and fighting violence against women. She is the Leader of the UC3M4Safety multidisciplinary team that proposes to use technology to protect women at the risk of sexual- or gender-based violence. The team has been a semifinalist in the International XPRIZE Women’s Safety Competition.

Dr. Lopez-Ongil was a recipient of the Vodafone Foundation Award “Connecting for Good” in 2019.